Journal of Applied Meteorology and Climatology

Response of the Sea-Breeze to Urbanization in the Pearl River Delta Region

--Manuscript Draft--

Manuscript Number:	JAMC-D-18-0081
Full Title:	Response of the Sea-Breeze to Urbanization in the Pearl River Delta Region
Article Type:	Article
Order of Authors:	Cheng You
	Jimmy Fung
	Waipo TSE
Manuscript Classifications:	2.072: Buoyancy; 8.104: Mesoscale models
Abstract:	The Pearl River Delta (PRD) region has undergone rapid urbanization since the 1980s, which has had significant effects on the sea-breeze circulation in this region. Because the sea-breeze plays an important role in pollutant transportation and convective initiation in the PRD region, it is meaningful to study the effects of urbanization on the sea-breeze. In this study, three numerical experiments were conducted from 2 June to 31 August 2010 with land-use data from 1988, 1999, and 2010. For each simulation, characteristics of the sea-breeze such as the start time, end time, intensity, height, pumping ability, and inland penetration distance were quantified. By comparing the characteristics of the sea-breeze in these simulations, its response to urbanization was quantified. The results show that urbanization enhances the duration, height, and intensity of the sea-breeze but blocks its inland penetration. One physical mechanism is proposed to dynamically elucidate the response of the sea-breeze to urbanization. Because the urban area in the PRD region is concentrated near the coast, urbanization imposes a positive heating gradient on the coastal region and a negative heating gradient on the region further inland. The positive heating gradient may intensify the sea-breeze, and the negative heating gradient may prevent the sea-breeze from propagating further inland.

Response of the Sea-Breeze to Urbanization in the Pearl River Delta Region

Cheng YOU [a], Jimmy Chi-Hung FUNG [a, b], Wai Po TSE [c]

[a] Division of Environment and Sustainability, The Hong Kong University of Science and Technology, Hong Kong

[b] Department of Mathematics, The Hong Kong University of Science and Technology, Hong Kong

[c] Environmental Science Programs, School of Science, The Hong Kong University of Science and Technology, Hong Kong

Abstract

The Pearl River Delta (PRD) region has undergone rapid urbanization since the 1980s, which has had significant effects on the sea-breeze circulation in this region. Because the sea-breeze plays an important role in pollutant transportation and convective initiation in the PRD region, it is meaningful to study the effects of urbanization on the sea-breeze.

In this study, three numerical experiments were conducted from 2 June to 31 August 2010 with land-use data from 1988, 1999, and 2010. For each simulation, characteristics of the sea-breeze such as the start time, end time, intensity, height, pumping ability, and inland penetration distance were quantified. By comparing the characteristics of the sea-breeze in these simulations, its response to urbanization was quantified. The results show that urbanization enhances the duration, height, and intensity of the sea-breeze but blocks its inland penetration.

Corresponding author. Cheng YOU, cheng.you@misu.su.se

One physical mechanism is proposed to dynamically elucidate the response of the sea-breeze to urbanization. Because the urban area in the PRD region is concentrated near the coast, urbanization imposes a positive heating gradient on the coastal region and a negative heating gradient on the region further inland. The positive heating gradient may intensify the sea-breeze, and the negative heating gradient may prevent the sea-breeze from propagating further inland.

Keywords: Sea-breeze · Solenoid Term · Frontogenesis Function · PRD Region · Urbanization

1 Introduction

The sea-breeze is fueled by land-sea thermal differences in coastal regions (Simpson 1994). With the extension of urban areas in coastal cities, the thermal properties of land surface are changed significantly, which may affect sea-breezes. Much attention has been dedicated to the effects of urbanization on sea-breezes. Ado (1992) found that an urban heat island near the coast can strengthen the sea-breeze in the growing stage. A sea-breeze from the East Sea and a lake-breeze from Lake Taihu were found to intensify the heat island circulation over Shanghai (You-hua 1998). A sea-breeze front can be more easily recognized with more urbanized land-use, but two additional hours are needed for the sea-breeze front to penetrate further inland (Lin et al. 2008). With the presence of an urban area, the propagation speed of the sea-breeze front may be slowed (Freitas et al. 2007; Leroyer et al. 2014). In the absence of the urban area, the head of the sea-breeze front in New York City would extend vertically to a much higher level (Thompson et al. 2007). Interaction among the sea-breeze, the Taipei urban heat island, and the mountains was found to strengthen thunderstorms downstream of the sea-breeze (Chen et al. 2007). Similar results have also been found in Houston and in central Taiwan (Shepherd et al. 2010; Lin et al. 2008).

The Pearl River Delta (PRD) region has undergone rapid urbanization since the 1980s. Several researchers have focused on the effects of urbanization on sea-breeze events in this region. It was found that industrial development and urbanization in the PRD region strengthens the daytime sea-breeze circulation (Lo et al. 2007). Lu (2010) found that the urbanization of Shenzhen may dramatically intensify the sea-breeze to the west of Hong Kong, and similar results were also found by Wu et al. (2011). However, most of these studies focused only on case studies, which cannot illustrate the general effects of urbanization on sea-breezes. In addition, these studies did not define any standard variables to quantify the onset time, cessation time, or strength of sea-breezes, which makes it difficult to quantitatively compare sea-breeze events in different land-use scenarios. In this study, a method to quantitatively characterize the sea-breeze is used to analyze and compare sea-breezes simulated from 2 June to 31 August in 2010, with land-use data from 1988, 1999, and 2010. More information about the simulation and the method is introduced in Section 2, and the statistical results are shown and discussed in Section 3. In Section 4, one physical mechanism is proposed to dynamically elucidate the response of the sea-breeze to urbanization in the PRD region. Section 5 then concludes the paper.

2 Data and Methods

As illustrated by Figure 1, the PRD region underwent rapid urbanization between 1988 and 2010, especially in Guangzhou, Foshan, Zhongshan, Dongguan, and Shenzhen, and the urban area is mostly concentrated in the coastal region. To identify the effects of urbanization on sea-breezes in the PRD region, three numerical experiments were conducted from 2 June to 31 August 2010 with land-use data from 1988, 1999, and 2010 (Figure 1). These simulations used domain settings designed by Xie et al. (2012). The weather research and forecasting terrain-following coordinate contains 47 eta levels, and 17 levels were within a height of 1 km. Asymmetric Convective Model Version 2 was used in this simulation, because it performs better than other planetary boundary layer schemes in the PRD region (Xie et al. 2012). For this simulation, the root-mean-square error of the 2-m temperature ranged from 1.87°C to 2.11°C, whereas it ranged from 1.39 to 1.51 m/s for a 10-m wind speed. The evaluation results showed that the overall performance of the weather research and forecasting model over the PRD region is reasonable with this configuration.

The method identified by (Cheng and Fung, 2017) was used to quantitatively characterize the sea-breeze in different land-use scenarios. As shown in Figure 2 (a), the three main coasts in the PRD region were simplified as straight lines AG, BC, and DE. We focused mainly on coasts AG and DE because coast BC has shifted considerably over the past 30 years. The horizontal wind field is decomposed into divergent and non-divergent parts with the method introduced by Cao and Xu (2011) and Xu et al. (2011). Along coasts AG and DE, the normal divergent velocity (V_D) and normal original velocity (V_O) were spatially averaged. Positive signals of V_D were taken as sea-breeze events along each coast if they began after sunrise and finished and appeared with a positive V_O. The start time of a sea-breeze was defined as the time at which V_D and V_O are both positive, whereas the time at which any of them will be negative was taken as the end time. V_D at a height of 50 m was taken as the intensity of the sea-breeze. In the averaged vertical wind field (Figure 2 (b)), the height at which the V_O over the coast first changes from positive to negative was considered as the height of the sea-breeze (H_{SB}). Integrated V_O over height (i.e., f_x) is also evaluated, and its zero contours are used to indicate the boundary of atmospheric circulation. The inland lateral boundary illustrated by f_x can also be used to estimate the inland penetration distance of the sea-breeze (D_{SB}). In addition, f_x at the height of H_{SB} over the coast (f_H) can also quantify the pumping ability of the sea-breeze circulation. f_H and H_{SB} were evaluated for separable sea-breeze events that have clear boundaries.

3 Statistical Results

3.1 Characteristics of Sea-Breeze along Coast AG with Different Land-Use Scenarios

Three numerical experiments with land-use data from 1988, 1999, and 2010 were designed to illustrate the effects of urbanization on the sea-breeze circulation. The method mentioned above was used to quantify the sea-breeze in the PRD region and statistical results are summarized in table 1. In Exp1, the average start time was 11:30, and the average end time was 17:20. The average start time of sea-breeze events in Exp2 was 35 min earlier than that of Exp1, and the end time was 45 min later. Therefore, the mean duration of the sea-breeze events in Exp2 was 80 min longer. The increased urban land-use in Exp2 and Exp3 appears to have enhanced the intensity of the sea-breeze events. In addition, the statistical results of Exp2 and Exp3 are quite similar.

Separable sea-breeze cases in these three experiments were selected with the method mentioned in Chapter 2; nine separable cases were found in Exp3 along with eight cases each in Exp1 and Exp2. Their characteristics are summarized in Table 2. With more urban land-use in Exp2 and Exp3, the height and pumping ability of the sea-breeze both appeared to be enhanced, but the inland penetration distance did not change as obviously. However, the average lateral boundary of the sea-breeze circulation in Exp1 reached further inland than that in Exp3 at the start time, the strongest time, and the end time. (Figure 8 only illustrates the boundary at the strongest time.) A similar phenomenon was also found by Freitas et al. (2007).

Urbanization can enhance sea-breezes and strengthen their pumping ability. At the start time, the vertical profiles of V_O and f_x in Exp3 almost overlap with those in Exp2, and both are larger than those in Exp1. In addition, the sea-breeze and sea-breeze circulation in Exp2 and Exp3 are lifted into higher levels. Similarly, at strongest time, V_O and f_H in Exp2 and Exp3 are larger than that in Exp1. For Exp2, urbanization apparently intensifies the near-surface sea-breeze, but the height of the sea-breeze and sea-breeze circulation remain the same as in Exp1. In Exp3, however, the sea-breeze and sea-breeze circulation are more than 100 m higher. The near-surface sea-breeze in Exp2 is slightly stronger than that in Exp3, whereas at a higher level, it is much smaller than that in Exp3. At the end time, with more urban land-use, the sea-breeze is more intensive from the ground to the top, in conjunction with its pumping ability. Meanwhile, the sea-breeze and sea-breeze circulation are also higher.

The vertical motion above the convergent zone can also be intensified by urbanization (Figure 4 (b) (d) (f)), and the vertical profile of the potential temperature becomes better mixed or even more unstable with more urban land-use (Figure 4 (a) (c) (e)). In addition, the height of the lifted inversion layer is also increased. At the start time, the vertical motion in Exp2 is not increased, and its profile of potential temperature is almost parallel with that in Exp1. In Exp3, however, the vertical motion is intensified dramatically. With stronger vertical motion, the near-surface layer in Exp3 becomes better mixed, and the height of the inversion layer is increased. At the strongest time, with a more urbanized PRD, the vertical motion intensifies in the convergent zone near coast AG. Meanwhile, the vertical profile of potential temperature in Exp2 is still nearly parallel with that in Exp3, whereas the near-surface potential temperature in Exp3 decreases slightly with height, and the inversion layer is lifted higher. Similarly, at the end time, the vertical motion increases and the atmospheric boundary layer becomes less stable as a result of urbanization in both Exp2 and

Exp3. For Exp3, a thin unstable layer can be found near the surface. In addition, at this moment, the lifted inversion layer in Exp3 is also higher than those in the other two numerical experiments.

3.2 Characteristics of Sea-Breeze along Coast DE with Different Land-Use Scenarios

Similar to coast AG, the intensity, height, and duration of sea-breeze events at coast DE are also enhanced by urbanization (Table 3). Their end time is also generally postponed by nearly 30 min, whereas with more urban land-use in Exp2 and 3, the start time of the sea-breeze is 12 min later than that in Exp1. Therefore, the duration is slightly increased, but not as dramatically as for coast AG. The general intensity of sea-breezes at 50 m is modulated by urbanization in a different manner from coast AG. The intensities in Exp1 and Exp2 change only slightly, where in Exp3 the intensity changes significantly.

The characteristics of separable sea-breeze events are summarized in Table 4. With more urban land-use, the sea-breeze along coast DE pumps more air from the sea to the land and extends vertically to a higher level. However, compared with Exp1, the inland penetration distances in Exp2 and Exp3 are shortened by urbanization. This effect is also supported by Figure 10, which illustrates that the lateral boundary of the sea-breeze in Exp1 is always located further inland than that in Exp3. The effects of urbanization on the vertical profile of the sea-breeze at coast *DE* are similar to those at coast *AG.* The difference is that the height of the inversion layer near coast *DE* is almost the same in each scenario.

4 Physical Mechanism to Modulate the Urbanization Effects on Sea-Breeze Circulation

To illustrate the effects of urbanization on the sea-breeze at coasts *DE* and *AG*, the potential temperature, pressure, solenoid term, atmospheric friction term, and vorticity acceleration were evaluated on the mean vertical cross-section (Figure 2 (a)) and averaged among all sea-breeze events at the start time, strongest time, and end time. The potential temperature gradient, solenoid term, and atmospheric friction term over the coast are greater at all moments in Exp3 than in Exp1; however, the pressure field changes little. The sea-breeze in Exp3 is higher than that in Exp1 at the start time and the strongest time, but the inland penetration distance in Exp3 is reduced, especially for the sea-breeze along coast *DE*. In Exp1 at coast *DE*, as they propagate gradually inland, the sea-breeze circulation and the mountain-valley circulation on the land develop into a new circulation on a larger horizontal scale (green line in Figure 10 (a)). At the end time, all three circulations (one sea-breeze circulation and two mountain-valley circulations) have combined into one. However, in Exp3, the average sea-breeze circulation (black line in Figure 10 (a)) does not merge with any other circulations, which shortens its inland penetration distance.

The physical mechanism of sea-breeze circulation proposed by Cheng and Fung (2017) is used in this section to explain this phenomenon. As concluded by Cheng and Fung (2017) , for the sea-breeze in the PRD region, the positive vorticity acceleration that stimulates sea-breeze circulation is mainly contributed by the solenoid term, which in turn is mostly controlled by the temperature gradient because the pressure gradient force is nearly constant during the development of the sea-breeze circulation.

Considering the importance of the temperature gradient, the frontogenesis function was thus used to diagnose the magnitude and spatial distribution of the four factors (FG1 to FG4) that contribute to the temperature gradient. FG1 and FG4 evaluate the effects of heterogeneous diabatic and adiabatic heating, respectively, on the temperature gradient, whereas FG2 and FG3 quantify the effects of convergence and deformation, respectively, on the temperature gradient. As discussed by Cheng and Fung (2017) , among these four factors, FG1 (diabatic heating) is the ultimate driving force of the sea-breeze circulation, and it can be offset by FG4 (adiabatic heating). Meanwhile, the sea-breeze can also be sustained by convergence and deformation in the convergent zone.

Frontogenesis functions were evaluated in the mean vertical cross-section along coast AG (Figure 2(a)). As shown in Figure 5, urbanization has significant effects on frontogenesis functions. With more urban land-use in Exp3, the diabatic heating and adiabatic cooling on the land is increased, whereas the adiabatic heating induced by the downward flow mainly above the sea is increased. Hence, the positive effects of FG1 on the temperature gradient are offset by the negative effects from FG4, and their overall effects (FG1 + FG4) are still enhanced by urbanization (Figure 6 (C)). The convergence and deformation effects (FG2 and FG3) from the offshore region to the convergent zone are apparently intensified (Figure 5 (B) (C)), which may contribute to enhancement of the temperature gradient and sea-breeze circulation there. Meanwhile, FG2 and FG3 among the inverse flow over the coastal region are decreased dramatically by urbanization. Similar results also can be found along coast *DE.*

Corresponding to the enhanced FG1 near coasts AG and DE in Exp3, the surface sensible heat flux is also increased there with greater urban land-use (Figure 7 and 9). Because the urban region is concentrated in the coastal region along these two coasts (Figure 7 (b) and 9 (b)), the surface sensible heat flux increases inland first and reaches its maximum at the most urbanized region (Figure 7 (e) and 9 (e)). It then shows an obvious decrease further inland. Therefore, a positive heating gradient is imposed from the coast to the most urbanized region, and the temperature gradient is thus increased (Figure 8 (a) and 10 (a)). However, a negative heating gradient is imposed on the region further inland; this negative gradient is conducive to the negative temperature gradient difference between Exp1 and Exp3 (Figure 8 (a) and 10 (a)), which could induce a negative solenoid difference between Exp1 and Exp3 (Figure 8 (b) and 10 (b)). This negative solenoid difference could intensify the development of anomalous negative vorticity acceleration that could stimulate a negative vortex in front of the sea-breeze circulation and suppress its inland propagation (Figure 8 (c) and 10 (c)). In contrast, the positive heating gradient over the coast increases the temperature gradient and hence intensifies the solenoid term there (Figure 8 (b) and 10 (b)). The enhanced solenoid term could offset the increased negative effects of atmospheric friction and contribute positively to vorticity acceleration (Figure 8 (c) and 10 (c)). Consequently, the sea-breeze circulation is intensified in Exp3.

5 Conclusions

In this study, three numerical experiments using land-use data from 1988, 1999, and 2010 were conducted to quantitatively characterize the response of the sea-breeze circulation to the rapid urbanization of the PRD region. The results show that with more urban land-use, the duration, height, pumping ability, and intensity of the sea-breeze are obviously enhanced, whereas its inland penetration distanced is shortened. In the convergent zone, vertical motion is intensified and the boundary layer becomes better mixed. In addition, the near-surface unstable layer is more obvious, and the inversion layer is lifted to a higher level. Because urban land-use in the PRD region is concentrated in coastal regions, from the coastal region to the most urbanized area, a positive heating gradient anomaly is imposed by urbanization, whereas a negative heating gradient anomaly can be found from the most urbanized area to somewhere further inland. This positive heating gradient anomaly in the coastal region contributes to the enhancement of FG1 and the temperature gradient. The increased temperature gradient strengthens the solenoid term and thus intensifies the vorticity acceleration, which could fuel sea-breeze circulation. The relationships among these variables are shown in Figure 11. However, a negative heating anomaly is conducive to a negative vorticity acceleration anomaly, which could prevent the sea-breeze circulation (positive vortex) from propagating further inland by stimulating one negative vortex immediately in front of the sea-breeze circulation.

Acknowledgement

We thank Dr. CAO Jie (Institution of Atmospheric Physics, CAS) and Prof. Qin XU (NOAA/National Severe Storms Laboratory, USA) for providing the source code of wind decomposition. We appreciate the assistance of the Hong Kong Observation (HKO), which provided the meteorological data. This work was supported by NSFC/RGC Grant N_HKUST631/05, NSFC-FD Grant U1033001, and the RGC Grant 16303416.

Reference

Ado, H. Y., 1992: Numerical study of the daytime urban effect and its interaction with the sea breeze. *J. Appl. Meteorol.*, **31**, 1146–1164.

Cao, J., and Q. Xu, 2011: Computing streamfunction and velocity potential in a limited domain of arbitrary shape. Part II: Numerical methods and test experiments. *Adv. Atmos. Sci.*, **28**, 1445–1458.

Chen, T.-C., S.-Y. Wang, and M.-C. Yen, 2007: Enhancement of afternoon thunderstorm activity by urbanization in a valley: Taipei. *J. Appl. Meteorol. Climatol.*, **46**, 1324–1340.

Freitas, E. D., C. M. Rozoff, W. R. Cotton, and P. L. S. Dias, 2007: Interactions of an urban heat island and sea-breeze circulations during winter over the metropolitan area of São Paulo, Brazil. *Boundary-Layer Meteorol.*, **122**, 43–65.

Leroyer, S., S. Belair, S. Z. Husain, and J. Mailhot, 2014: Subkilometer Numerical Weather Prediction in an Urban Coastal Area: A Case Study over the Vancouver Metropolitan Area. *J. Appl. Meteorol. Climatol.*, **53**, 1433–1453, doi:10.1175/jamc-d-13-0202.1.

Lin, C.-Y., F. Chen, J. C. Huang, W.-C. Chen, Y.-A. Liou, W.-N. Chen, and S.-C. Liu, 2008: Urban heat island effect and its impact on boundary layer development and land–sea circulation over northern Taiwan. *Atmos. Environ.*, **42**, 5635–5649.

Lo, J. C. F., A. K. H. Lau, F. Chen, J. C. H. Fung, and K. K. M. Leung, 2007: Urban modification in a mesoscale model and the effects on the local circulation in the Pearl River Delta region. *J. Appl. Meteorol. Climatol.*, **46**, 457–476.

Lu, X., K. C. Chow, T. Yao, A. K. H. Lau, and J. C. H. Fung, 2010: Effects of urbanization on the land sea breeze circulation over the Pearl River Delta region in winter. *Int. J. Climatol.*, **30**, 1089–1104, doi:10.1002/joc.1947.

Shepherd, J. M., M. Carter, M. Manyin, D. Messen, and S. Burian, 2010: The impact of urbanization on current and future coastal precipitation: a case study for Houston. *Environ.*

Plan. B Plan. Des., **37**, 284–304.

Simpson, J. E., 1994: *Sea breeze and local winds*. Cambridge University Press,.

Thompson, W. T., T. Holt, and J. Pullen, 2007: Investigation of a sea breeze front in an urban environment. *Q. J. R. Meteorol. Soc.*, **133**, 579–594.

Wu, J.-B., K.-C. Chow, J. C. H. Fung, A. K. H. Lau, and T. Yao, 2011: Urban heat island effects of the Pearl River Delta city clusters—their interactions and seasonal variation. *Theor. Appl. Climatol.*, **103**, 489–499.

Xie, B., J. C. H. Fung, A. Chan, and A. Lau, 2012: Evaluation of nonlocal and local planetary boundary layer schemes in the WRF model. *J. Geophys. Res. Atmos.*, **117**.

Xu, Q., J. Cao, and S. Gao, 2011: Computing streamfunction and velocity potential in a limited domain of arbitrary shape. Part I: Theory and integral formulae. *Adv. Atmos. Sci.*, **28**, 1433–1444.

You-hua, M. M. T., 1998: INTERACTION BETWEEN SEA AND LAND BREEZE AND HEAT ISLAND CIRCULATION DURING THE SUMMER OVER THE DELTA REGION OF THE YANGTZE RIVER AND URBANIZATION EFFECT ON CLIMATE [J]. *Plateau Meteorol.*, **3**.

Cheng Y., Fung JCH, 2017: Characteristics of sea-breeze circulation in the Pearl River Delta region and its mechanism of development. (Submitted to Boundary-layer Meteorology)

Table 1. Average start time, end time, duration, and intensity of sea-breeze events along coast AG in numerical experiments with different land-use data.

Numerical Experiment	Exp1 (1988)	Exp2 (1999)	Exp3 (2010)
Start Time	11:30	10:55	10:50
End Time	17:20	18:05	17:50
Duration	5 h 50 min	7 h 10 min	7 h
Intensity (m/s)	2.26	2.51	2.47

Table 2. Number of separable cases, average inland penetration distance (D_{SB}), pumping ability (f_H), and height (H_{SB}).

Numerical Experiment	Exp1	Exp2	Exp3
Number of Separable Cases	16	16	16
Inland Penetration Distance (km)	14.6	15	16.7
Pumping Ability (m^3/s)	904	966	1277
Height (m)	466	525	628

Table 3. Average start time, end time, duration, and intensity of sea-breeze events along coast DE in numerical experiments with different land-use data.

Numerical Experiment	Exp1	Exp2	Exp3
Start Time	10:30	10:42	10:42
End Time	16:55	17:23	17:26
Duration	6 h 25 min	6 h 41 min	6 h 44 min
Intensity (m/s)	1.97	1.98	2.14

Table 4. Number of separable cases, average inland penetration distance (D_{SB}), height (H_{SB}), and pumping ability (f_H).

Numerical Experiment	Exp1	Exp2	Exp3
Number of separable cases	21	23	24
Inland Penetration distance (km)	14.0	11.0	12.7
Pumping Ability (m^3/s)	574	622	691
Height (m)	412	433	460

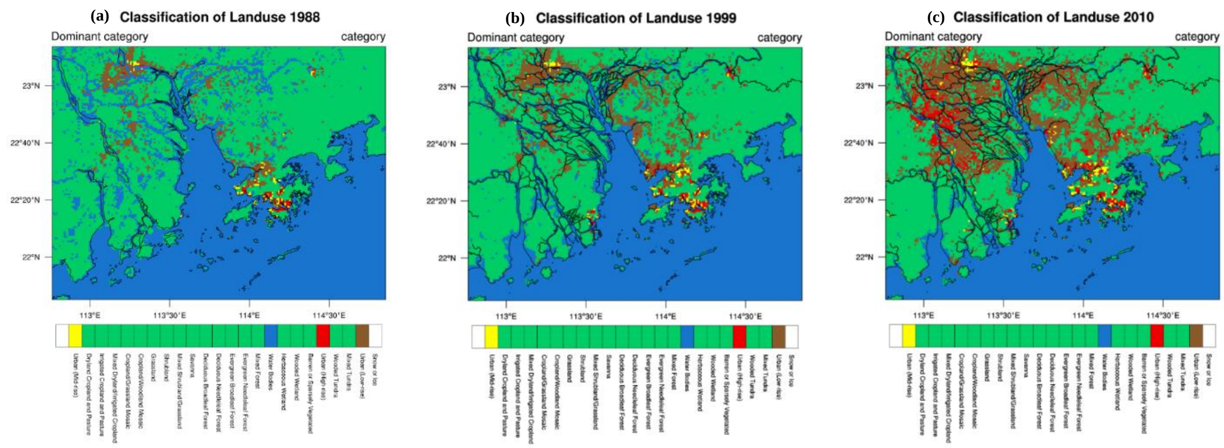

Figure 1. Land-use by category in 1988 (a), 1999 (b), and 2010 (c).

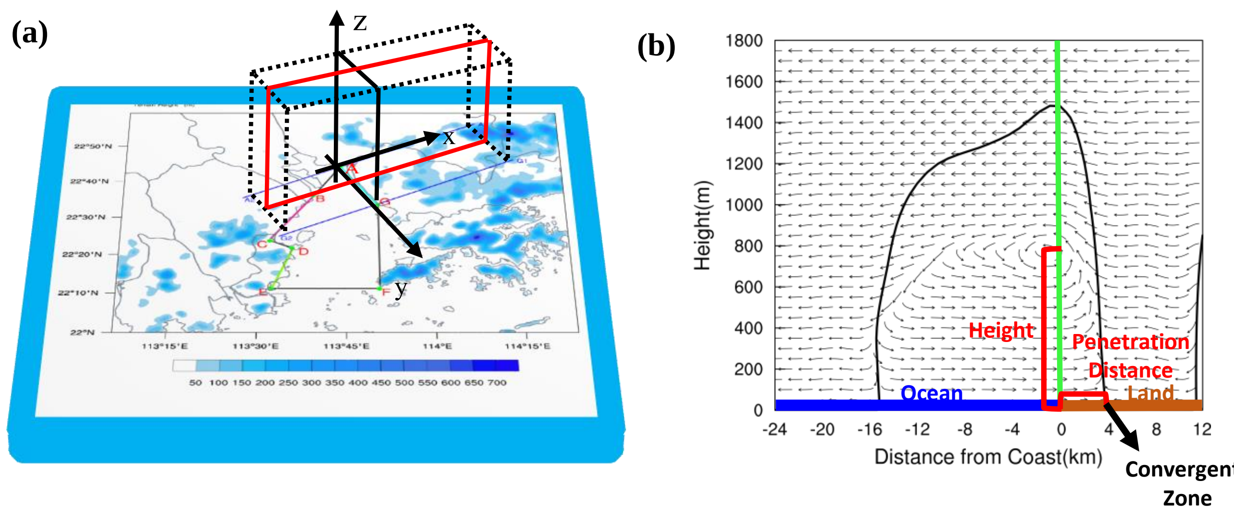

Figure 2. (a) Terrain and coastlines in the PRD region. Coastlines are simplified into straight lines AG, DE, and BC. In this study, most variables related to coast AG were evaluated in the Cartesian coordinate system designed in Figure 2 (a). Its y-axis coincides with coast AG, and the x-axis overlaps line A_1A_2. We focused mainly on variables on the mean vertical cross-section (red rectangle in Figure 2 (a)), which is achieved by averaging the three-dimensional physical variables in the black box over the y direction. Using the wind field in Figure 2 (b) as an example shows the average sea-breeze circulation in the mean vertical cross-section along coast AG. The same method was also used for coast DE.

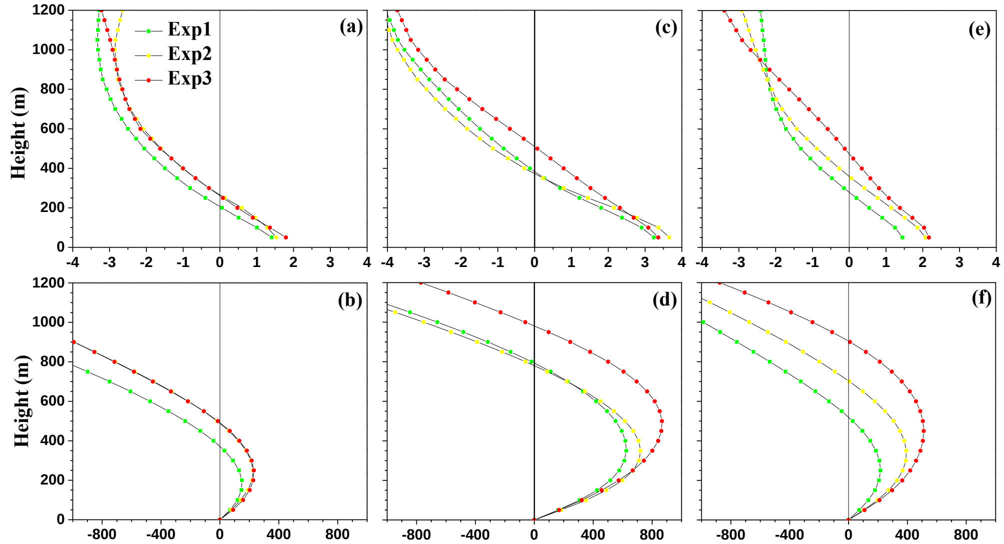

Figure 3. Average vertical profile of V_O in m/s (a) (c) (e) and f_x in m^3/s (b) (d) (f) in Exp1, Exp2, and Exp3 over coast AG at the start time (a) (b), the strongest time (c) (d), and the end time (e) (f). The maximum value of f_x is f_H.

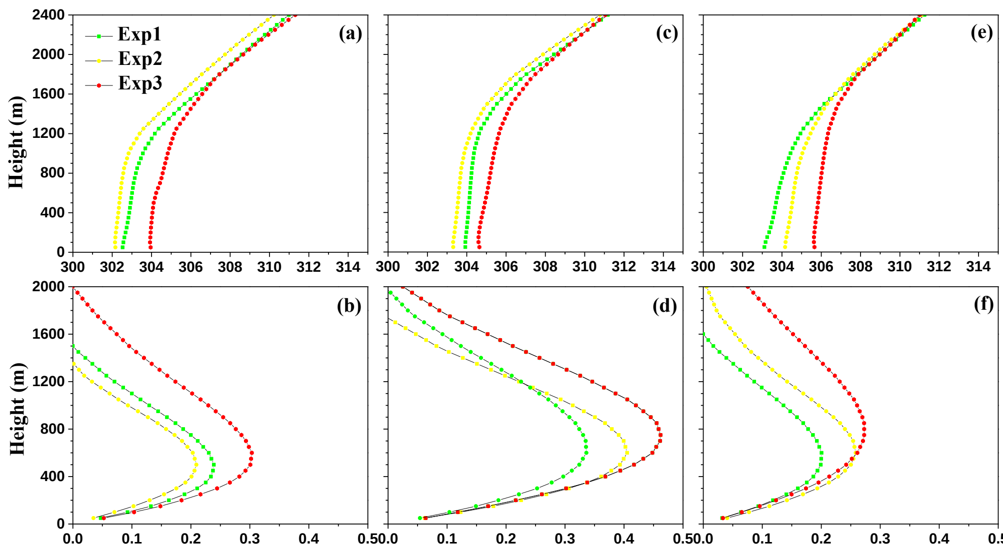

Figure 4. Average vertical profile of vertical velocity (W) (in m/s) (a) (c) (e) and potential temperature (T_p) (in K) (b) (d) (f) in Exp1, Exp2, and Ex3 over convergent zone near coast AG at the start time (a) (b), the strongest time (c)(d), and the end time (e) (f).

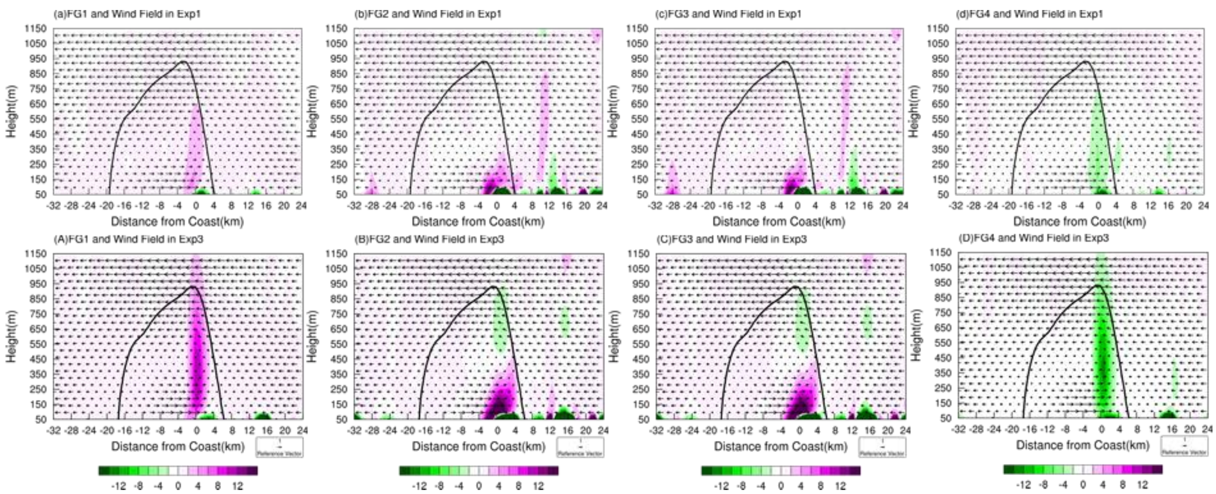

Figure 5. Average FG1 (a), FG2 (b), FG3 (c), and FG4 (d) along coast AG in Exp1. FG1 and FG4 are given in $10^{-11} \cdot k \cdot m^{-1} \cdot s^{-1}$, and FG2 and FG3 are given in $10^{-12} \cdot k \cdot m^{-1} \cdot s^{-1}$. The thick black line is the zero contour of the stream function, which can approximate the boundary of the sea-breeze circulation. (A) through (D) are similar to (a) through (d) but they are for FG1 (A), FG2 (B), FG3 (C), and FG4 (D) along coast AG in Exp3.

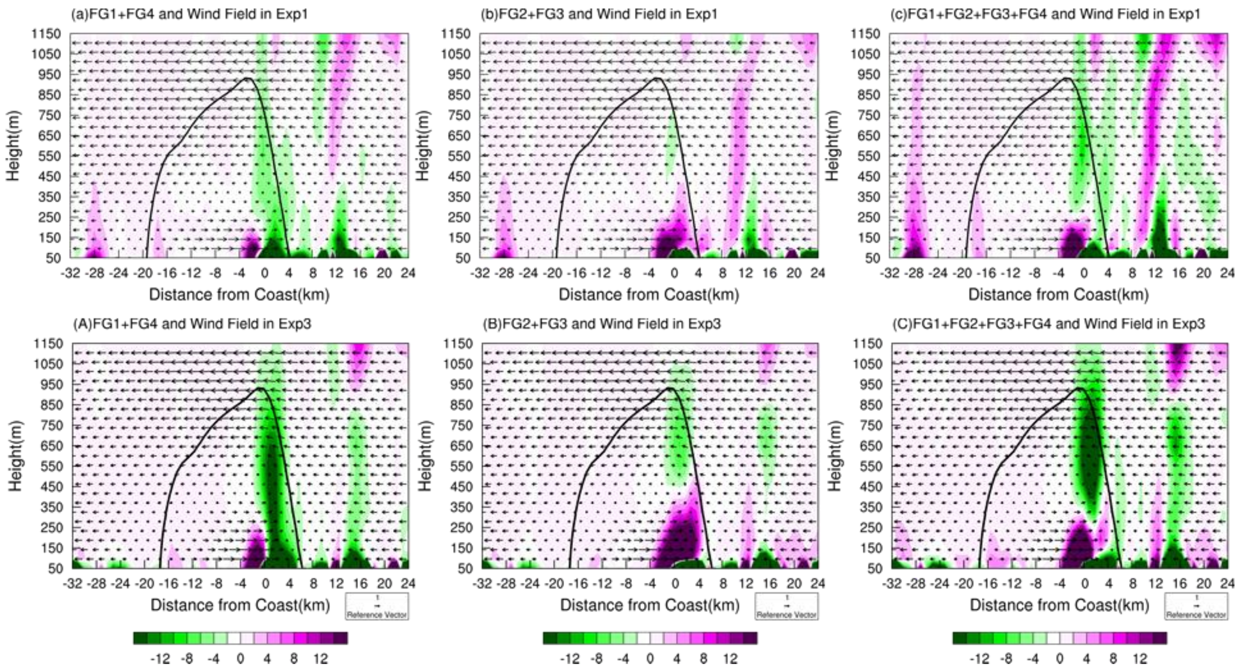

Figure 6. Average FG1+FG4 (a), FG2+FG3 (b), and FG1+FG2+FG3+FG4 (c) along coast AG in Exp1. FG1+FG4 and FG1+FG2+FG3+FG4 are given in $10^{-11} \cdot k \cdot m^{-1} \cdot s^{-1}$, and FG2+FG3 is given in $10^{-12} \cdot k \cdot m^{-1} \cdot s^{-1}$. The thick black line is the zero contour of the stream function, which can approximate the boundary of the sea-breeze circulation. (A) through (C) are similar to (a) through (c) but they are for FG1+FG4 (A), FG2+FG3 (B), and FG1+FG2+FG3+FG4 (C) along coast AG in Exp3.

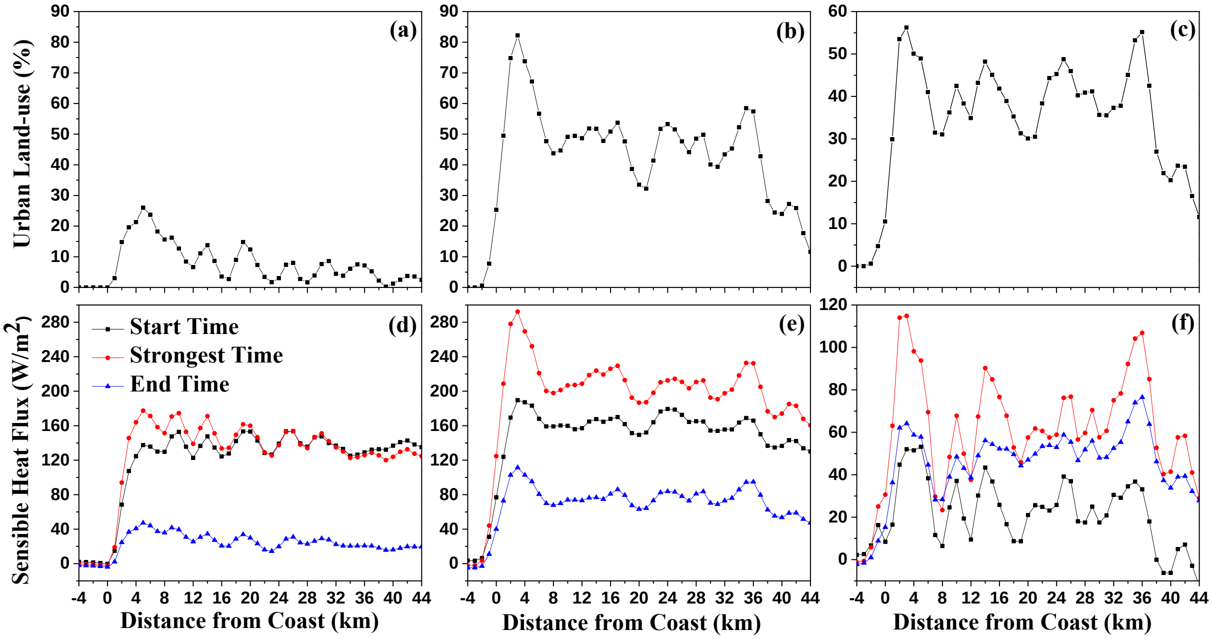

Figure 7. (a) (b): Relative area of urban land-use near coast AG in Exp1 and Exp3. (d) (e): Average surface sensible heat flux (w/m^2) near coast AG at start time (black line), strongest time (red line), and end time (blue line) in Exp1 (d) and Exp3 (e). The difference between (a) and (b) is shown in (c), and the difference between (d) and (e) is shown in (f).

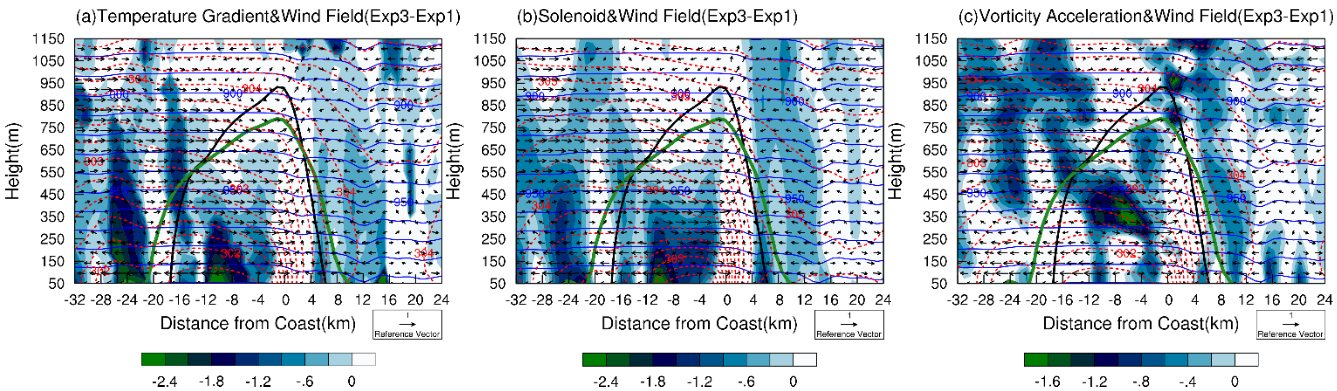

Figure 8. Color-filled contours show (a) the temperature gradient difference ($10^{-6}\ k/m$) between Exp1 and Exp3 at the strongest time, (b) the solenoid difference ($10^{-7}\ s^{-2}$) between Exp1 and Exp3, and (c) the vorticity acceleration difference ($10^{-7}\ s^{-2}$) between Exp1 and Exp3. The wind field in (a) through (c) is the difference (m/s) between the average wind field in Exp1 and Exp3. In (a) (c), blue line shows average pressure contours in Exp1, and red line shows potential temperature contours in Exp1, whereas the blue line in (b) shows average pressure contours in Exp3, and the red line shows average potential temperature contours in Exp1. The thick green line shows the average boundary of sea-breeze circulation in Exp1, and the black line shows the average boundary of sea-breeze circulation in Exp3.

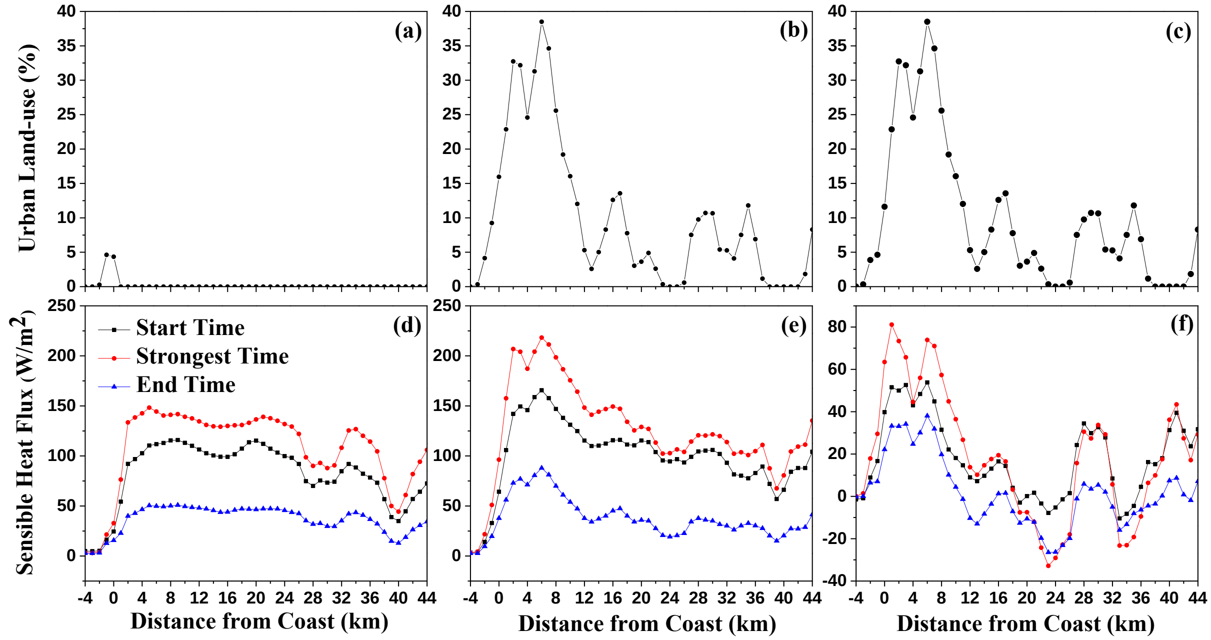

Figure 9. Similar to Figure 7, but for coast DE.

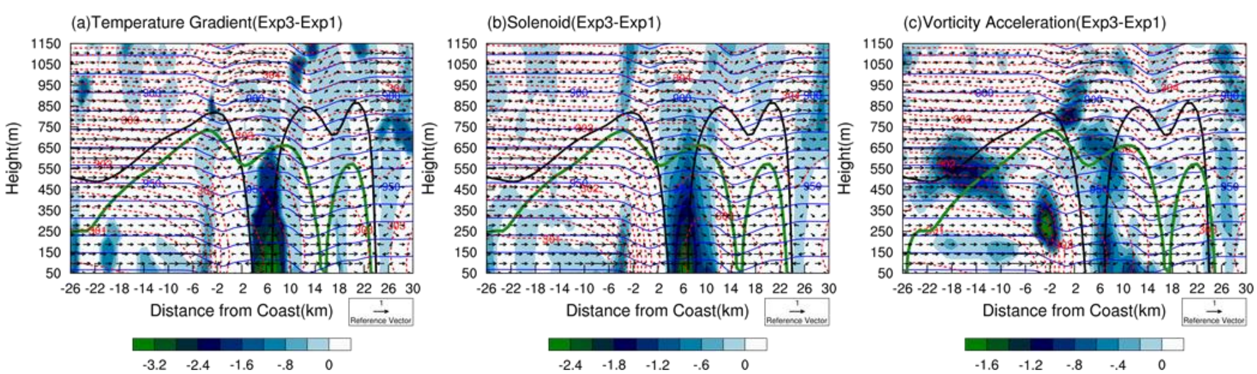

Figure 10. Similar to Figure 8, but for coast DE.

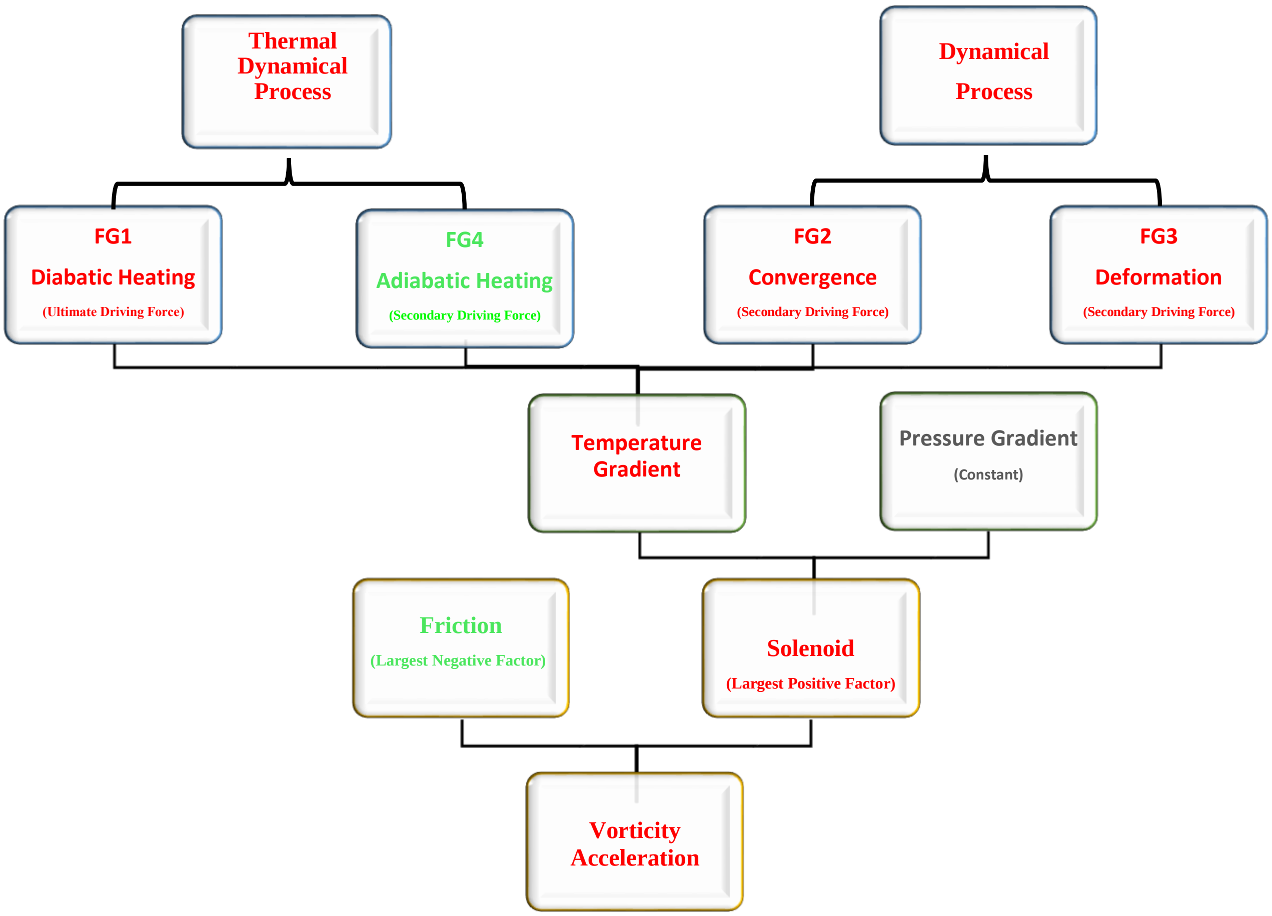

Figure 11. Flow chart of the relationship between the variables used to diagnose the dynamic process of sea-breeze circulation in this study.